

Weak Ferromagnetism in Altermagnets from Alternating g -Tensor Anisotropy

Daegeun Jo,^{1,2,*} Dongwook Go,³ Yuriy Mokrousov,^{3,4}
Peter M. Oppeneer,^{1,2} Sang-Wook Cheong,^{5,†} and Hyun-Woo Lee^{6,‡}

¹*Department of Physics and Astronomy, Uppsala University, P.O. Box 516, SE-75120 Uppsala, Sweden*

²*Wallenberg Initiative Materials Science for Sustainability, Uppsala University, SE-75120 Uppsala, Sweden*

³*Institute of Physics, Johannes Gutenberg University Mainz, 55099 Mainz, Germany*

⁴*Peter Grünberg Institut and Institute for Advanced Simulation, Forschungszentrum Jülich and JARA, 52425 Jülich, Germany*

⁵*Rutgers Center for Emergent Materials and Department of Physics and Astronomy,
Rutgers University, Piscataway, New Jersey 08854, USA*

⁶*Department of Physics, Pohang University of Science and Technology, Pohang 37673, Korea*

(Dated: October 24, 2024)

Altermagnets are magnetic materials with antiferromagnetic spin ordering but exhibit ferromagnetic properties. Understanding the microscopic origin of the latter is a central problem. Ferromagnet-like properties such as the anomalous Hall effect are linked with weak ferromagnetism, whose microscopic origin in altermagnets remains unclear however. We show theoretically that the alternating g -tensor anisotropy in altermagnets can induce weak ferromagnetism even when the Dzyaloshinskii-Moriya interaction is forbidden. We demonstrate this mechanism for both collinear and noncollinear spin altermagnets and explain various properties of the weak ferromagnetism in altermagnets. Our findings provide insights for characterizing and manipulating magnetic configurations in altermagnets.

Magnetic materials have traditionally been categorized by spin ordering: ferromagnets (FMs) with parallel spins and antiferromagnets (AFMs) with antiparallel spins. However, recent studies [1–20] have highlighted the significant role of the interplay between spin ordering and local crystal structure surrounding magnetic atoms in characterizing magnetic materials. This insight has led to the classification of a new type of magnetism, dubbed altermagnetism [19–23]. Altermagnets (AMs) have antiferromagnetic spin ordering with alternating local crystal structures at sublattices. In view of the symmetry analysis based on the spin group theory, the alternating local crystal structure is crucial for the FM-like properties of the AMs. First of all, the electronic bands are spin-split [24–26]. In the presence of SOC, they can exhibit further FM-like behavior such as the magneto-optical effect [14, 27] and the anomalous Hall effect [5, 28, 29]. Therefore, AMs offer potential for novel spintronic applications [30–32], combining the benefits of both FMs [33, 34] and AFMs [35, 36].

Despite FM-like behavior being compatible with symmetry, a fundamental question still remains unanswered: What is a *microscopic* defining feature of AMs that distinguishes them from conventional AFMs and gives rise to their FM-like behavior? Recently, ferroic ordering of magnetic octupoles has been proposed as a microscopic order parameter to describe d -wave AMs [37]. According to a Landau theory augmented by spin-space symmetries, this magnetic octupole can couple linearly to the magnetic dipole through SOC [38], enabling weak ferromagnetism (WFM) in AMs [38–42] and their FM-like behavior. However, the microscopic origin of WFM in AMs remains unclear. Although the Dzyaloshinskii-Moriya interaction (DMI) [43, 44] can induce the WFM in some

AMs such as α -Fe₂O₃ [44] and La₂CuO₄ [45], it cannot explain the substantial orbital magnetization of rutile-type [5, 14] and Mn₃Sn-type [46, 47] AMs predicted by first-principles calculations, necessitating deeper investigation into the origin of the WFM in AMs.

In this Letter, we study a thus far unexplored origin of WFM in AMs: alternating g -tensor anisotropy. The g -tensor not only characterizes the spin exchange energy but also reflects the structural anisotropy, prompting us to examine its role in AMs. We demonstrate theoretically that the alternation of the g -tensor anisotropy among sublattices of AMs can naturally lead to WFM, primarily driven by the orbital moment, even when the DMI is forbidden. A wide range of AMs exhibit this phenomenon either intrinsically (type-I AMs) or under strain (type-II AMs) [42]. This mechanism extends beyond conventional AMs with collinear spin ordering and straightforwardly applies to AMs with noncollinear spin ordering [42]. Our findings not only provide insights into FM-like properties of AMs but also offer a fresh perspective on previous studies of WFM in various compounds [43–51].

The spectroscopic g -tensor [52] is defined as the ratio of the total magnetic moment to the spin angular momentum, which can be represented by a 3×3 matrix \mathbf{g} . In many high-symmetry systems, principal axes can be chosen such that the orbital and spin angular momenta are aligned with them. In this case, \mathbf{g} can be expressed as a diagonal matrix with elements

$$g_\alpha = 2 + \frac{\langle L_\alpha \rangle}{\langle S_\alpha \rangle}, \quad (1)$$

where $\langle L_\alpha \rangle$ and $\langle S_\alpha \rangle$ are expectation values of orbital and spin angular momentum operators \mathbf{L} and \mathbf{S} along the principal axis α , respectively. For example, let us

consider a FM exhibiting the spin S_0 along the α -axis in the absence of SOC, where the orbital is quenched. When weak SOC is taken into account, a finite $\langle L_\alpha \rangle$ is induced, which is linear in the SOC strength λ_{SO} [53]. On the other hand, the spin-orbit correction to the spin is at least second-order [47], i.e., $\langle S_\alpha \rangle = S_0 + O(\lambda_{\text{SO}}^2)$. Therefore, in the weak SOC regime, the SOC-induced magnetic moment originates primarily from the orbital moment, causing g_α to deviate from 2 by an amount proportional to the induced orbital moment or λ_{SO} [48].

The anisotropic orbital moment is an essential ingredient of our discussion. If the crystal structure is anisotropic, the spin-orbit-induced orbital moment depends on the spin exchange field direction $\hat{\mathbf{s}}$ due to the interplay between spin and crystal structure, which is also known to be responsible for magnetic anisotropy energy [53]. Here, we focus on its influence on the g -tensor anisotropy. Consider a magnetic atom subject to an electrical potential featuring uniaxial anisotropy with principal axes $\hat{\mathbf{e}}_\parallel$ and $\hat{\mathbf{e}}_\perp$, as illustrated in Fig. 1(a). We compare two configurations where orbital and spin angular momenta, aligning with $\hat{\mathbf{s}}$, are oriented either along $\hat{\mathbf{e}}_\parallel$ or $\hat{\mathbf{e}}_\perp$. Based on the previous discussion, we expect that the orbital angular momenta $L_\parallel \neq L_\perp$ are linearly proportional to the SOC strength, while the spin angular momenta S_\parallel and S_\perp remain approximately equal to the nonrelativistic value S_0 . Consequently, the g -tensor can be expressed as $\mathbf{g} = \text{diag}(g_\perp, g_\perp, g_\parallel)$, where $g_{\parallel(\perp)} \approx 2 + L_{\parallel(\perp)}/S_0$. This leads us to define the g -tensor anisotropy Δg as [54]:

$$\Delta g \equiv g_\parallel - g_\perp \approx \frac{L_\parallel - L_\perp}{S_0}. \quad (2)$$

Although we have assumed a ferromagnetic atom, our discussion can be generalized to altermagnetic systems by defining the g -tensor locally for each magnetic atom.

Now, we show that Δg combines with the alternating local crystal structure to generate the WFM of AMs. For illustration, we consider a prototypical altermagnetic system. The i -th magnetic atom is surrounded by a crystalline potential with uniaxial anisotropy, having principal axes $\hat{\mathbf{e}}_\parallel^i$ and $\hat{\mathbf{e}}_\perp^i$, as illustrated in Fig. 1(b). The local spin $\langle \mathbf{S}^i \rangle = S_0 \hat{\mathbf{s}}^i$ makes an angle ϕ_i with $\hat{\mathbf{e}}_\parallel^i$, satisfying $\sum_i^N \hat{\mathbf{s}}^i = 0$, where N is the number of magnetic atoms in a unit cell. The local g -tensor $\mathbf{g}^i = \text{diag}(g_\perp, g_\perp, g_\parallel)$ is defined in terms of the principal axes at each site. g_\parallel and g_\perp are independent of the sublattice, provided that the local crystal structures at each site are connected by rotational symmetry to each other [e.g., Figs. 1(c)-1(e)]. Thus, the total magnetic moment $\mathbf{m}_{\text{tot}} = -(\mu_B/\hbar) \sum_i^N \mathbf{g}^i \cdot \langle \mathbf{S}^i \rangle$ of this system is proportional to $\sum_i^N [g_\parallel \cos \phi_i \hat{\mathbf{e}}_\parallel^i + g_\perp (\hat{\mathbf{s}}^i - \cos \phi_i \hat{\mathbf{e}}_\parallel^i)]$ and given

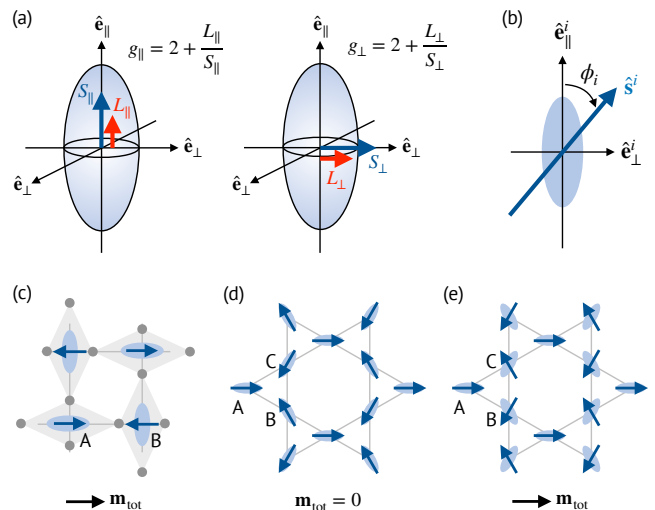


FIG. 1. (a) Schematic illustration of the g -tensor anisotropy for a magnetic atom. The blue ellipsoids illustrate uniaxial anisotropy. The unit vectors $\hat{\mathbf{e}}_\parallel$ and $\hat{\mathbf{e}}_\perp$ represent principal axes parallel and perpendicular to the axis of the highest symmetry, respectively. S_\parallel and S_\perp (L_\parallel and L_\perp) are the spin (orbital) angular momenta along $\hat{\mathbf{e}}_\parallel$ and $\hat{\mathbf{e}}_\perp$, respectively. (b) Example of the local structure of the magnetic sublattice i in an AM. (c)-(e) Altermagnetic systems with alternating g -tensor anisotropy. Panels (c) and (e) exhibit the WFM (type-I AM), while panel (d) does not (type-II AM).

by

$$\mathbf{m}_{\text{tot}} = -\frac{\mu_B}{\hbar} \Delta g S_0 \mathbf{s}_\parallel, \quad \mathbf{s}_\parallel = \sum_i^N \cos \phi_i \hat{\mathbf{e}}_\parallel^i, \quad (3)$$

to first-order in SOC. Equation (3) is the main result of our paper, which clearly demonstrates that the net magnetic moment of AMs is proportional to Δg instead of the electron spin g -factor 2 for strong FMs. It is worth noting that the direction of \mathbf{m}_{tot} is determined by \mathbf{s}_\parallel , representing the projection of spins with respect to local crystalline axes. Since \mathbf{m}_{tot} in Eq. (3) is dominated by the orbital contribution, it is naturally related to orbital-dominated anomalous Hall AFMs [47, 55]. We emphasize that our mechanism of WFM works even when the DMI is forbidden [Fig. 1(c)] and instead requires alternating local crystal structure. It is thus distinct from WFM due to the DMI [43, 44] or single-ion anisotropy [48], which does not require the alternating local crystal structure. The latter mechanisms disregard the orbital moment and therefore do not fully explain the orbital-dominated WFM in RuO_2 reported by first-principles calculations [5, 14].

Here, we examine AMs with collinear spins using Eq. (3). Figure 1(c) shows a two-dimensional square lattice consisting of two magnetic atoms A and B with opposite spins. The gray circles at the corners of diamonds

represent the nonmagnetic atoms, which give rise to the anisotropic crystal potential depicted by blue ellipses. Similar types of structures are commonly found in rutile-type AMs, such as RuO_2 [5], MnF_2 [6], and NiF_2 [48]. For an arbitrary in-plane spin configuration with $\phi_A = \phi$ and $\phi_B = \phi + \pi/2$, Eq. (3) leads to

$$\mathbf{m}_{\text{tot}} = -\frac{\mu_B}{\hbar} \Delta g S_0 (\cos \phi \hat{\mathbf{x}} - \sin \phi \hat{\mathbf{y}}). \quad (4)$$

Interestingly, the predicted $\mathbf{m}_{\text{tot}} \parallel \mathbf{p} = \cos \phi \hat{\mathbf{x}} - \sin \phi \hat{\mathbf{y}}$ can be either parallel or perpendicular to the Néel vector $\hat{\mathbf{n}} = \cos \phi \hat{\mathbf{x}} + \sin \phi \hat{\mathbf{y}}$ depending on ϕ . This angular dependence is consistent with first-principles calculation for RuO_2 [5, 14]. Such AMs exhibiting WFM have been categorized as type-I AMs [42]. Conversely, for the out-of-plane spin configuration with $\hat{\mathbf{s}}^i = \pm \hat{\mathbf{z}}$ (e.g., CoF_2 [56]), implying $\phi_A = \phi_B$, Eq. (3) yields $\mathbf{m}_{\text{tot}} = 0$ since the relevant g -tensor anisotropy in this configuration is the difference between two g_{\perp} 's. Inducing difference between them by strain can induce net magnetization, which amounts to piezomagnetism [56, 57]. This type of AMs, with zero net magnetization and piezomagnetism, has been categorized as type-II AMs [42].

Next, we test the above predictions by performing tight-binding calculations for a two-dimensional square lattice consisting of two magnetic atoms A and B with an antiferromagnetic spin ordering described by an angle ϕ [Fig. 2(a)]. The wavefunctions are described by d_{xy} , d_{yz} and d_{zx} atomic orbitals for each atom. The tight-binding Hamiltonian \mathcal{H} for magnetic atoms is formally written as:

$$\begin{aligned} \mathcal{H} = & \sum_{\langle i,j \rangle, m, n, \sigma} t_{ij, mn} c_{i m \sigma}^{\dagger} c_{j n \sigma} \\ & - \frac{J_{\text{sd}}}{\hbar} \sum_{i, n, \sigma, \sigma'} \hat{\mathbf{s}}^i \cdot \mathbf{c}_{i n \sigma}^{\dagger} \mathbf{S}_{\sigma \sigma'} c_{i n \sigma'} \\ & + \frac{\lambda_{\text{SO}}}{\hbar^2} \sum_{i, m, n, \sigma, \sigma'} c_{i m \sigma}^{\dagger} \mathbf{L}_{mn} \cdot \mathbf{S}_{\sigma \sigma'} c_{i n \sigma'}. \end{aligned} \quad (5)$$

Here, $c_{i n \sigma}^{\dagger}$ ($c_{i n \sigma}$) is the creation (annihilation) operator of an electron at site i with orbital index $n = xy, yz, zx$ and spin $\sigma = \uparrow, \downarrow$. The first term of \mathcal{H} describes electron hopping between the nearest-neighbor site pairs $\langle i, j \rangle$. The hopping parameter $t_{ij, mn}$ is determined using the Slater-Koster method [58] with parameters t_{σ} , t_{π} , and t_{δ} , which represent σ -, π -, and δ -bonding between d orbitals, respectively. In this model, only t_{π} is assumed to be nonzero for the sake of simplicity. The second term corresponds to the exchange interaction between a conduction electron spin \mathbf{S} and the molecular field $(J_{\text{sd}}/\hbar)\hat{\mathbf{s}}^i$. The third term describes the atomic SOC, where the matrix elements of \mathbf{L} are locally defined in terms of the atomic orbital basis. Note that this lattice does not contain nonmagnetic atoms in contrast to typical rutile-structure AMs [e.g., Fig. 1(c)]. Thus, Eq. (5) reflects neither local anisotropy nor altermagnetism. To capture the

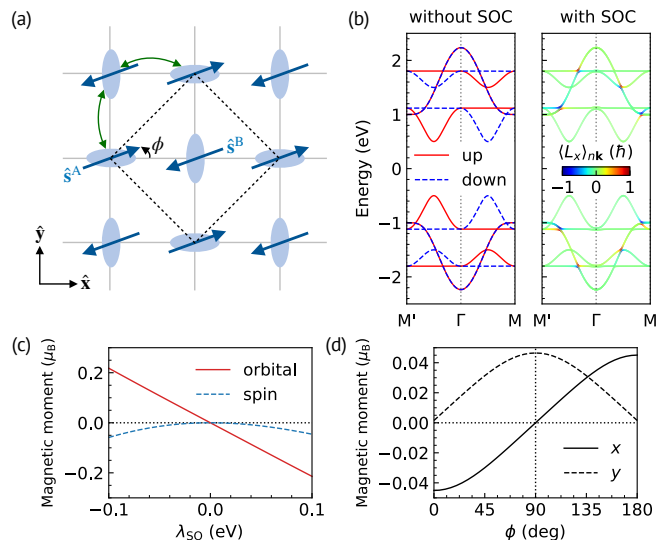


FIG. 2. (a) Schematic illustration of the tight-binding model \mathcal{H} for an AM with collinear spins. The dashed lines represent the unit cell, and the green arrows indicate the nearest-neighbor hoppings. The blue ellipses display the anisotropy. (b) Band structures without (left panel) and with (right panel) SOC. (c) The net orbital and spin magnetic moments at the Fermi energy $E_F = -0.9$ eV as a function of the SOC strength λ_{SO} . (d) x - and y -components of the total magnetic moment at $E_F = -0.9$ eV depending on the spin angle ϕ .

alternating local crystal structure arising from the non-magnetic atoms, we introduce the sublattice-dependent crystal field to each magnetic atom as follows:

$$\mathcal{H}_{\text{CF}} = \sum_{i, n, \sigma} \Delta_{in} c_{i n \sigma}^{\dagger} c_{i n \sigma}, \quad (6)$$

where $\Delta_{i, xy} = 0$ and $\Delta_{i, yz} = -\Delta_{i, zx} \equiv \tau \Delta_{\text{CF}}/2$ with the sublattice index τ being $+1$ (-1) for A(B). This term leads to the alternating local anisotropy, as depicted by Fig. 2(a), thereby giving rise to altermagnetism.

Figure 2(b) shows the band structures without (left) and with (right) SOC for the total Hamiltonian $\mathcal{H} + \mathcal{H}_{\text{CF}}$ with $t_{\pi} = 0.5$ eV, $J_{\text{sd}} = 1.0$ eV, $\phi = 0$, $\lambda_{\text{SO}} = 0.02$ eV, and $\Delta_{\text{CF}} = 1.0$ eV. The nonrelativistic spin splitting alternates in sign between the \mathbf{k} paths from Γ to $M = (0.5, 0.5)$ and from Γ to $M' = (-0.5, 0.5)$. With SOC, doubly degenerate d_{xy} bands hybridize with d_{zx} bands, inducing an orbital angular momentum $\langle L_x \rangle_{n\mathbf{k}}$ for each \mathbf{k} point with band n . The anisotropy of $\langle L_x \rangle_{n\mathbf{k}}$ in \mathbf{k} space results in the net orbital moment, which is linear in λ_{SO} [Fig. 2(c)] and dominant over the net spin moment that is quadratic in λ_{SO} . These features agree with our expectations. Additionally, the ϕ dependence of \mathbf{m}_{tot} [Fig. 2(d)] is consistent with Eq. (4).

We examine the connection between the g -tensor anisotropy and net magnetic moment. For this, we first calculate the orbital (spin) angular momentum projected onto atoms A and B, denoted by $\langle L_x^A \rangle$ and $\langle L_x^B \rangle$

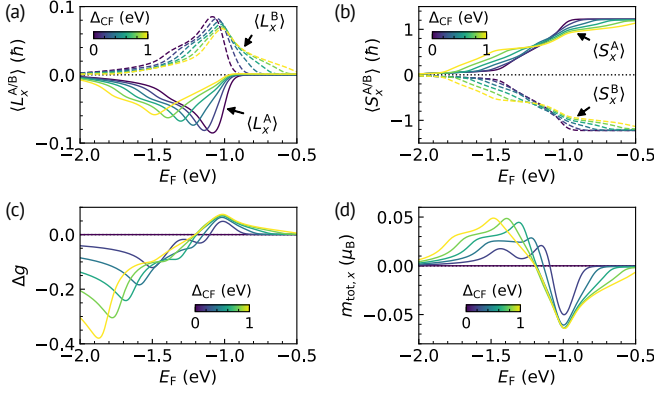


FIG. 3. (a),(b) Fermi energy (E_F) dependences of (a) orbital and (b) spin angular momenta for atom A (solid lines) and atom B (dashed lines) with varying crystal field parameter Δ_{CF} . (c),(d) E_F dependences of (c) g -tensor anisotropy Δg and (d) total magnetic moment $m_{tot,x}$ with varying Δ_{CF} .

($\langle S_x^A \rangle$ and $\langle S_x^B \rangle$), respectively, as a function of the Fermi energy E_F and as a function of the alternating crystal field parameter Δ_{CF} in \mathcal{H}_{CF} . Figure 3(a) demonstrates that $\langle L_x^A \rangle + \langle L_x^B \rangle$ is zero for $\Delta_{CF} = 0$ and becomes larger in magnitude as Δ_{CF} increases. In contrast, $\langle S_x^A \rangle + \langle S_x^B \rangle$ remains almost zero regardless of Δ_{CF} [Fig. 3(b)]. Then, the g -tensor anisotropy, evaluated by $\Delta g = \langle L_x^A \rangle / \langle S_x^A \rangle - \langle L_x^B \rangle / \langle S_x^B \rangle$, gradually increases with Δ_{CF} [Fig. 3(c)]. Note that the total magnetic moment [Fig. 3(d)] exhibits a clear correlation with Δg . Moreover, we find that the product $\Delta g(|\langle S_x^A \rangle| + |\langle S_x^B \rangle|)/2$ exhibits the essentially identical variation as $m_{tot,x}$ with respect to E_F or Δ_{CF} change, providing further support to Eq. (3).

Next, we extend our theory to AMs with noncollinear spin structures [42]. For example, Fig. 1(d) displays a kagome lattice with a triangular structure where the spins of sublattices A, B, and C are each rotated by 120 degrees relative to one another and the local g -tensor of each sublattice is anisotropic. In this case, the angles between spin and g -tensor's principal axis are identical for all sublattices, i.e., $\phi_A = \phi_B = \phi_C$, which makes \mathbf{m}_{tot} in Eq. (3) zero (type-II AM). On the other hand, for an inverse triangular structure [Fig. 1(e)], where the spins are rotated by -120 degrees, Eq. (3) predicts a nonvanishing \mathbf{m}_{tot} (type-I AM). For arbitrary angles, $\phi_A = \phi$, $\phi_B = \phi + 2\pi/3$, and $\phi_C = \phi + 4\pi/3$, \mathbf{m}_{tot} follows Eq. (4) [55].

We also examine these predictions numerically by applying \mathcal{H} for the kagome lattices in Figs. 1(d) and 1(e). Since the magnetic atoms themselves in the kagome lattices give rise to the alternating local crystal structure, we consider in our calculation only \mathcal{H} , which describes the magnetic atoms, and ignore \mathcal{H}_{CF} , which describes the effect of nonmagnetic atoms implicitly. For each magnetic atom, the atomic orbitals $d_{3z^2-r^2}$, d_{yz} , and d_{zx} are taken

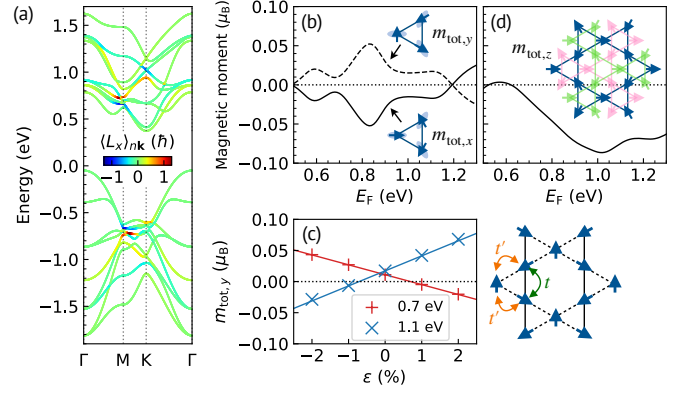


FIG. 4. (a) Band structure of the kagome lattice having an inverse triangular spin structure with $\phi = 0$. (b) Fermi energy (E_F) dependences of the net magnetic moment $m_{tot,x}$ for $\phi = 0$ (solid line) and $m_{tot,y}$ for $\phi = \pi/2$ (dashed line). The insets display the spin configuration for the three sublattices. (c) $m_{tot,y}$ of the distorted kagome lattice (right panel) at $E_F = 0.7$ eV (red + symbols) and $E_F = 1.1$ eV (blue x symbols) with varying strain parameter ε . Solid lines indicate a linear relation between ε and $m_{tot,y}$. (d) E_F dependence of $m_{tot,z}$ for the bulk system with ABC-stacked kagome planes. The inset shows the top view of the structure, where blue, pink, and green layers are stacked in order.

into account. The following parameters are assumed: $t_\sigma = -1.0$ eV, $t_\pi = 0.5$ eV, $t_\delta = -0.1$ eV, $J_{sd} = 0.7$ eV, and $\lambda_{SO} = 0.02$ eV. The angles between the x -axis and the spins for atoms A, B, and C are given by ϕ , $\phi \pm 2\pi/3$, and $\phi \pm 4\pi/3$, respectively, where the signs indicate normal (+) [Fig. 1(d)] and inverse (-) [Fig. 1(e)] triangular spin structures. We first consider the latter structure. Its band structure for $\phi = 0$ [Fig. 4(a)] shows band-resolved $\langle L_x \rangle_{nk}$ summed over three sublattices A, B, and C. Analogous to the collinear spin case, \mathbf{m}_{tot} is dominated by the orbital contribution. In Fig. 4(b), the solid and dashed lines present the x - and y -components of \mathbf{m}_{tot} for $\phi = 0$ (e.g., Mn_3Ge and Mn_3Ga) and $\phi = \pi/2$ (e.g., Mn_3Sn), respectively. Note that they follow the predicted relation $m_{tot,x}(\phi) = -m_{tot,y}(\phi + \pi/2)$ [Eq. (4)].

Motivated by an experiment [59] on the piezomagnetic properties of the kagome lattice with the inverse triangular spin structure, we examine the strain effect on \mathbf{m}_{tot} . The right panel of Fig. 4(c) shows a distorted kagome lattice, with solid and dashed lines indicating different bond lengths r and r' , respectively. Suppose $r' = (1 + \varepsilon)r$ due to strain with the parameter ε . The hopping parameter modified by strain can be approximately written as $t'_{ij,mn} = t_{ij,mn}/(1 + \varepsilon)^2$ [60], where $t_{ij,mn}$ is the original hopping parameter. To describe this system, we construct the tight-binding model using $t_{ij,mn}$ and $t'_{ij,mn}$ for different bonds, while preserving the lattice structure. Figure 4(c) presents $m_{tot,y}$ at $E_F = 0.7$ eV and $E_F = 1.1$ eV, demonstrating a piezomagnetic effect [56]: magnetization is induced by strain linearly. As \mathbf{m}_{tot} for $\varepsilon = 0$

is tiny, \mathbf{m}_{tot} can be easily switched by the piezomagnetic effect, in qualitative agreement with the experiment [59].

For the normal triangular spin structure [Fig. 1(d)], our numerical calculation finds $\mathbf{m}_{\text{tot}} = 0$, as predicted by Eq. (3). However, WFM can be induced via symmetry-breaking stacking. For instance, the structures of Mn_3Rh , Mn_3Ir , and Mn_3Pt consist of kagome planes with ABC-type stacking along the (111) direction [61, 62], which breaks the C_{2x} symmetry. To examine these systems, we apply \mathcal{H} to the three-dimensional bulk structure composed of ABC-stacked kagome lattices with the normal triangular spin structure [inset of Fig. 4(d)]. In this system, the off-diagonal g -tensor element $g_{zx} = \langle L_z + 2S_z \rangle / \langle S_x \rangle$ becomes nonzero due to the broken C_{2x} symmetry. As a result, out-of-plane magnetization is induced, as shown in Fig. 4(d). Our analysis based on the g -tensor explains previous studies on kagome materials [46, 47, 49, 50, 61, 63] with a fresh mechanism in terms of altermagnetism.

In conclusion, we have demonstrated that WFM can be induced in AMs by the alternating g -tensor anisotropy Δg , which is a distinguishing feature of AMs that sets them apart from conventional AFMs. Δg may be experimentally evaluated from the ferromagnetic resonance spectroscopy [54]. This mechanism applies to AMs with either collinear or noncollinear spin structures. The concept of Δg is useful for classifying type-I and type-II AMs, and understanding the emergence of WFM with broken symmetries, thereby providing valuable insights for characterizing and manipulating magnetic configurations in various AMs. We suggest further investigations on its role in novel AMs with twisted [64, 65], Janus [65–67], or supercell [68] structures. Δg is intimately related to the orbital degree of freedom [69, 70] and presents a promising research direction toward orbital engineering in AMs.

D.J. and P.M.O. were supported by the Swedish Research Council (VR), the Knut and Alice Wallenberg Foundation (Grants No. 2022.0079 and 2023.0336), and the Wallenberg Initiative Materials Science for Sustainability (WISE) funded by the Knut and Alice Wallenberg Foundation. D.G., Y.M., and P.M.O. acknowledge funding from the European Union’s HORIZON EUROPE, under the grant agreement No 101129641, and D.G. and Y.M. acknowledge financial support by the Deutsche Forschungsgemeinschaft (DFG, German Research Foundation)–TRR 288–422213477 (project B06), and TRR 173/3–268565370 (project A11). S.-W.C. was supported by the DOE under Grant No. DOE:DE-FG02-07ER46382. H.-W.L. was supported by the Samsung Science and Technology Foundation (Grant No. BA-1501-51) and the National Research Foundation of Korea (NRF) (No. RS-2024-00356270, RS-2024-00410027). The calculations were supported by resources provided by the National Academic Infrastructure for Supercomputing in Sweden (NAISS) at NSC Linköping,

partially funded by VR through Grant No. 2022-06725.

* daegeun.jo@physics.uu.se

† sange@physics.rutgers.edu

‡ hwl@postech.ac.kr

- [1] Y. Noda, K. Ohno, and S. Nakamura, Momentum-dependent band spin splitting in semiconducting MnO_2 : a density functional calculation, *Physical Chemistry Chemical Physics* **18**, 13294 (2016).
- [2] K.-H. Ahn, A. Hariki, K.-W. Lee, and J. Kuneš, Antiferromagnetism in RuO_2 as d -wave Pomeranchuk instability, *Phys. Rev. B* **99**, 184432 (2019).
- [3] M. Naka, S. Hayami, H. Kusunose, Y. Yanagi, Y. Motome, and H. Seo, Spin current generation in organic antiferromagnets, *Nature Communications* **10**, 4305 (2019).
- [4] S. Hayami, Y. Yanagi, and H. Kusunose, Momentum-Dependent Spin Splitting by Collinear Antiferromagnetic Ordering, *Journal of the Physical Society of Japan* **88**, 123702 (2019).
- [5] L. Šmejkal, R. González-Hernández, T. Jungwirth, and J. Sinova, Crystal time-reversal symmetry breaking and spontaneous Hall effect in collinear antiferromagnets, *Science Advances* **6**, eaaz8809 (2020).
- [6] L.-D. Yuan, Z. Wang, J.-W. Luo, E. I. Rashba, and A. Zunger, Giant momentum-dependent spin splitting in centrosymmetric low- Z antiferromagnets, *Phys. Rev. B* **102**, 014422 (2020).
- [7] S. Hayami, Y. Yanagi, and H. Kusunose, Bottom-up design of spin-split and reshaped electronic band structures in antiferromagnets without spin-orbit coupling: Procedure on the basis of augmented multipoles, *Phys. Rev. B* **102**, 144441 (2020).
- [8] H. Reichlová, R. L. Seeger, R. González-Hernández, I. Kounta, R. Schlitz, D. Kriegner, P. Ritzinger, M. Lamme, M. Leiviskä, V. Petříček, P. Doležal, E. Schmoranzarová, A. Bad’ura, A. Thomas, V. Baltz, L. Michez, J. Sinova, S. T. B. Goennenwein, T. Jungwirth, and L. Šmejkal, Macroscopic time reversal symmetry breaking by staggered spin-momentum interaction (2021), arXiv:2012.15651 [cond-mat.mes-hall].
- [9] L.-D. Yuan, Z. Wang, J.-W. Luo, and A. Zunger, Prediction of low- Z collinear and noncollinear antiferromagnetic compounds having momentum-dependent spin splitting even without spin-orbit coupling, *Phys. Rev. Mater.* **5**, 014409 (2021).
- [10] M. Naka, Y. Motome, and H. Seo, Perovskite as a spin current generator, *Phys. Rev. B* **103**, 125114 (2021).
- [11] R. González-Hernández, L. Šmejkal, K. Výborný, Y. Yanagi, J. Sinova, T. Jungwirth, and J. Železný, Efficient Electrical Spin Splitter Based on Nonrelativistic Collinear Antiferromagnetism, *Phys. Rev. Lett.* **126**, 127701 (2021).
- [12] H.-Y. Ma, M. Hu, N. Li, J. Liu, W. Yao, J.-F. Jia, and J. Liu, Multifunctional antiferromagnetic materials with giant piezomagnetism and noncollinear spin current, *Nature Communications* **12**, 2846 (2021).
- [13] L.-D. Yuan, Z. Wang, J.-W. Luo, and A. Zunger, Strong influence of nonmagnetic ligands on the momentum-dependent spin splitting in antiferromagnets, *Phys. Rev. B* **103**, 224410 (2021).

- [14] X. Zhou, W. Feng, X. Yang, G.-Y. Guo, and Y. Yao, Crystal chirality magneto-optical effects in collinear antiferromagnets, *Phys. Rev. B* **104**, 024401 (2021).
- [15] S. A. Egorov, D. B. Litvin, and R. A. Evarestov, Antiferromagnetism-Induced Spin Splitting in Systems Described by Magnetic Layer Groups, *The Journal of Physical Chemistry C* **125**, 16147 (2021).
- [16] I. I. Mazin, K. Koepnik, M. D. Johannes, R. González-Hernández, and L. Šmejkal, Prediction of unconventional magnetism in doped FeSb₂, *Proceedings of the National Academy of Sciences* **118**, e2108924118 (2021).
- [17] D.-F. Shao, S.-H. Zhang, M. Li, C.-B. Eom, and E. Y. Tsymlal, Spin-neutral currents for spintronics, *Nature Communications* **12**, 7061 (2021).
- [18] L. Šmejkal, A. B. Hellenes, R. González-Hernández, J. Sinova, and T. Jungwirth, Giant and Tunneling Magnetoresistance in Unconventional Collinear Antiferromagnets with Nonrelativistic Spin-Momentum Coupling, *Phys. Rev. X* **12**, 011028 (2022).
- [19] L. Šmejkal, J. Sinova, and T. Jungwirth, Beyond Conventional Ferromagnetism and Antiferromagnetism: A Phase with Nonrelativistic Spin and Crystal Rotation Symmetry, *Phys. Rev. X* **12**, 031042 (2022).
- [20] L. Šmejkal, J. Sinova, and T. Jungwirth, Emerging Research Landscape of Altermagnetism, *Phys. Rev. X* **12**, 040501 (2022).
- [21] I. Mazin (The PRX Editors), Editorial: Altermagnetism—A New Punch Line of Fundamental Magnetism, *Phys. Rev. X* **12**, 040002 (2022).
- [22] H. Chen, L. Liu, X. Zhou, Z. Meng, X. Wang, Z. Duan, G. Zhao, H. Yan, P. Qin, and Z. Liu, Emerging Antiferromagnets for Spintronics, *Advanced Materials* **36**, 2310379 (2024).
- [23] L. Bai, W. Feng, S. Liu, L. Šmejkal, Y. Mokrousov, and Y. Yao, Altermagnetism: Exploring New Frontiers in Magnetism and Spintronics (2024), arXiv:2406.02123 [cond-mat.mtrl-sci].
- [24] O. Fedchenko, J. Minár, A. Akashdeep, S. W. D'Souza, D. Vasilyev, O. Tkach, L. Odenbreit, Q. Nguyen, D. Kutnyakhov, N. Wind, L. Wenthaus, M. Scholz, K. Rossnagel, M. Hoesch, M. Aeschlimann, B. Stadtmüller, M. Kläui, G. Schönhense, T. Jungwirth, A. B. Hellenes, G. Jakob, L. Šmejkal, J. Sinova, and H.-J. Elmers, Observation of time-reversal symmetry breaking in the band structure of altermagnetic RuO₂, *Science Advances* **10**, eadj4883 (2024).
- [25] J. Krempaský, L. Šmejkal, S. W. D'Souza, M. Hajaoui, G. Springholz, K. Uhlířová, F. Alarab, P. C. Constantinou, V. Strocov, D. Usanov, W. R. Pudelko, R. González-Hernández, A. Birk Hellenes, Z. Jansa, H. Reichlová, Z. Šobáň, R. D. Gonzalez Betancourt, P. Wadley, J. Sinova, D. Kriegner, J. Minár, J. H. Dil, and T. Jungwirth, Altermagnetic lifting of Kramers spin degeneracy, *Nature* **626**, 517 (2024).
- [26] Y.-P. Zhu, X. Chen, X.-R. Liu, Y. Liu, P. Liu, H. Zha, G. Qu, C. Hong, J. Li, Z. Jiang, X.-M. Ma, Y.-J. Hao, M.-Y. Zhu, W. Liu, M. Zeng, S. Jayaram, M. Lenger, J. Ding, S. Mo, K. Tanaka, M. Arita, Z. Liu, M. Ye, D. Shen, J. Wrachtrup, Y. Huang, R.-H. He, S. Qiao, Q. Liu, and C. Liu, Observation of plaid-like spin splitting in a noncoplanar antiferromagnet, *Nature* **626**, 523 (2024).
- [27] A. Hariki, A. Dal Din, O. J. Amin, T. Yamaguchi, A. Badura, D. Kriegner, K. W. Edmonds, R. P. Cam-
pion, P. Wadley, D. Backes, L. S. I. Veiga, S. S. Dhesi, G. Springholz, L. Šmejkal, K. Výborný, T. Jungwirth, and J. Kuneš, X-Ray Magnetic Circular Dichroism in Altermagnetic α -MnTe, *Phys. Rev. Lett.* **132**, 176701 (2024).
- [28] L. Šmejkal, A. H. MacDonald, J. Sinova, S. Nakatsuji, and T. Jungwirth, Anomalous Hall antiferromagnets, *Nature Reviews Materials* **7**, 482 (2022).
- [29] Z. Feng, X. Zhou, L. Šmejkal, L. Wu, Z. Zhu, H. Guo, R. González-Hernández, X. Wang, H. Yan, P. Qin, X. Zhang, H. Wu, H. Chen, Z. Meng, L. Liu, Z. Xia, J. Sinova, T. Jungwirth, and Z. Liu, An anomalous Hall effect in altermagnetic ruthenium dioxide, *Nature Electronics* **5**, 735 (2022).
- [30] A. Bose, N. J. Schreiber, R. Jain, D.-F. Shao, H. P. Nair, J. Sun, X. S. Zhang, D. A. Muller, E. Y. Tsymlal, D. G. Schlom, and D. C. Ralph, Tilted spin current generated by the collinear antiferromagnet ruthenium dioxide, *Nature Electronics* **5**, 267 (2022).
- [31] H. Bai, L. Han, X. Y. Feng, Y. J. Zhou, R. X. Su, Q. Wang, L. Y. Liao, W. X. Zhu, X. Z. Chen, F. Pan, X. L. Fan, and C. Song, Observation of Spin Splitting Torque in a Collinear Antiferromagnet RuO₂, *Phys. Rev. Lett.* **128**, 197202 (2022).
- [32] S. Karube, T. Tanaka, D. Sugawara, N. Kadoguchi, M. Kohda, and J. Nitta, Observation of Spin-Splitter Torque in Collinear Antiferromagnetic RuO₂, *Phys. Rev. Lett.* **129**, 137201 (2022).
- [33] I. Žutić, J. Fabian, and S. Das Sarma, Spintronics: Fundamentals and applications, *Rev. Mod. Phys.* **76**, 323 (2004).
- [34] A. Hirohata, K. Yamada, Y. Nakatani, I.-L. Prejbeanu, B. Diény, P. Pirro, and B. Hillebrands, Review on spintronics: Principles and device applications, *Journal of Magnetism and Magnetic Materials* **509**, 166711 (2020).
- [35] T. Jungwirth, X. Marti, P. Wadley, and J. Wunderlich, Antiferromagnetic spintronics, *Nature Nanotechnology* **11**, 231 (2016).
- [36] V. Baltz, A. Manchon, M. Tsoi, T. Moriyama, T. Ono, and Y. Tserkovnyak, Antiferromagnetic spintronics, *Rev. Mod. Phys.* **90**, 015005 (2018).
- [37] S. Bhowal and N. A. Spaldin, Ferroically Ordered Magnetic Octupoles in d -Wave Altermagnets, *Phys. Rev. X* **14**, 011019 (2024).
- [38] P. A. McClarty and J. G. Rau, Landau theory of altermagnetism, *Phys. Rev. Lett.* **132**, 176702 (2024).
- [39] K. P. Kluczyk, K. Gas, M. J. Grzybowski, P. Skupiński, M. A. Borysiewicz, T. Fał, J. Suffczyński, J. Z. Domagala, K. Graszka, A. Mycielski, M. Baj, K. H. Ahn, K. Výborný, M. Sawicki, and M. Gryglas-Borysiewicz, Coexistence of Anomalous Hall Effect and Weak Net Magnetization in Collinear Antiferromagnet MnTe (2023), arXiv:2310.09134 [cond-mat.mes-hall].
- [40] C. Autieri, R. M. Sattigeri, G. Cuono, and A. Fakhredine, Dzyaloshinskii-Moriya interaction inducing weak ferromagnetism in centrosymmetric altermagnets and weak ferrimagnetism in noncentrosymmetric altermagnets (2023), arXiv:2312.07678 [cond-mat.mtrl-sci].
- [41] M. Milivojević, M. Orozović, S. Picozzi, M. Gmitra, and S. Stavrić, Interplay of altermagnetism and weak ferromagnetism in two-dimensional RuF₄ (2024), arXiv:2401.15424 [cond-mat.mtrl-sci].
- [42] S.-W. Cheong and F.-T. Huang, Altermagnetism with non-collinear spins, *npj Quantum Materials* **9**, 13 (2024).

- [43] I. Dzyaloshinsky, A thermodynamic theory of “weak” ferromagnetism of antiferromagnetics, *Journal of Physics and Chemistry of Solids* **4**, 241 (1958).
- [44] T. Moriya, Anisotropic Superexchange Interaction and Weak Ferromagnetism, *Phys. Rev.* **120**, 91 (1960).
- [45] S.-W. Cheong, J. D. Thompson, and Z. Fisk, Metamagnetism in La_2CuO_4 , *Phys. Rev. B* **39**, 4395 (1989).
- [46] J. Kübler and C. Felser, Non-collinear antiferromagnets and the anomalous Hall effect, *Europhysics Letters* **108**, 67001 (2014).
- [47] H. Chen, T.-C. Wang, D. Xiao, G.-Y. Guo, Q. Niu, and A. H. MacDonald, Manipulating anomalous Hall antiferromagnets with magnetic fields, *Phys. Rev. B* **101**, 104418 (2020).
- [48] T. Moriya, Theory of Magnetism of NiF_2 , *Phys. Rev.* **117**, 635 (1960).
- [49] S. Tomiyoshi and Y. Yamaguchi, Magnetic Structure and Weak Ferromagnetism of Mn_3Sn Studied by Polarized Neutron Diffraction, *Journal of the Physical Society of Japan* **51**, 2478 (1982).
- [50] T. Nagamiya, S. Tomiyoshi, and Y. Yamaguchi, Triangular spin configuration and weak ferromagnetism of Mn_3Sn and Mn_3Ge , *Solid State Communications* **42**, 385 (1982).
- [51] C. Ederer and N. A. Spaldin, Weak ferromagnetism and magnetoelectric coupling in bismuth ferrite, *Phys. Rev. B* **71**, 060401(R) (2005).
- [52] C. Kittel, On the Gyromagnetic Ratio and Spectroscopic Splitting Factor of Ferromagnetic Substances, *Phys. Rev.* **76**, 743 (1949).
- [53] P. Bruno, Tight-binding approach to the orbital magnetic moment and magnetocrystalline anisotropy of transition-metal monolayers, *Phys. Rev. B* **39**, 865 (1989).
- [54] L. Alahmed, X. Zhang, J. Wen, Y. Xiong, Y. Li, L.-c. Zhang, F. Lux, F. Freimuth, M. Mahdi, Y. Mokrousov, V. Novosad, W.-K. Kwok, D. Yu, W. Zhang, Y. S. Lee, and P. Li, Evidence of Magnon-Mediated Orbital Magnetism in a Quasi-2D Topological Magnon Insulator, *Nano Letters* **22**, 5114 (2022).
- [55] N. Ito and K. Nomura, Anomalous Hall Effect and Spontaneous Orbital Magnetization in Antiferromagnetic Weyl Metal, *Journal of the Physical Society of Japan* **86**, 063703 (2017).
- [56] T. Moriya, Piezomagnetism in CoF_2 , *Journal of Physics and Chemistry of Solids* **11**, 73 (1959).
- [57] A. S. Disa, M. Fechner, T. F. Nova, B. Liu, M. Först, D. Prabhakaran, P. G. Radaelli, and A. Cavalleri, Polarizing an antiferromagnet by optical engineering of the crystal field, *Nature Physics* **16**, 937 (2020).
- [58] J. C. Slater and G. F. Koster, Simplified LCAO Method for the Periodic Potential Problem, *Phys. Rev.* **94**, 1498 (1954).
- [59] M. Ikhlas, S. Dasgupta, F. Theuss, T. Higo, S. Kittaka, B. J. Ramshaw, O. Tchernyshyov, C. W. Hicks, and S. Nakatsuji, Piezomagnetic switching of the anomalous Hall effect in an antiferromagnet at room temperature, *Nature Physics* **18**, 1086 (2022).
- [60] W. A. Harrison, *Electronic structure and the properties of solids* (Dover, New York, 1989).
- [61] H. Chen, Q. Niu, and A. H. MacDonald, Anomalous Hall Effect Arising from Noncollinear Antiferromagnetism, *Phys. Rev. Lett.* **112**, 017205 (2014).
- [62] Y. Zhang, Y. Sun, H. Yang, J. Železný, S. P. P. Parkin, C. Felser, and B. Yan, Strong anisotropic anomalous Hall effect and spin Hall effect in the chiral antiferromagnetic compounds Mn_3X ($X = \text{Ge}, \text{Sn}, \text{Ga}, \text{Ir}, \text{Rh}, \text{and Pt}$), *Phys. Rev. B* **95**, 075128 (2017).
- [63] S. Nakatsuji, N. Kiyohara, and T. Higo, Large anomalous Hall effect in a non-collinear antiferromagnet at room temperature, *Nature* **527**, 212 (2015).
- [64] R. He, D. Wang, N. Luo, J. Zeng, K.-Q. Chen, and L.-M. Tang, Nonrelativistic Spin-Momentum Coupling in Antiferromagnetic Twisted Bilayers, *Phys. Rev. Lett.* **130**, 046401 (2023).
- [65] S. Sheoran and S. Bhattacharya, Nonrelativistic spin splittings and altermagnetism in twisted bilayers of centrosymmetric antiferromagnets, *Phys. Rev. Mater.* **8**, L051401 (2024).
- [66] I. Mazin, R. González-Hernández, and L. Šmejkal, Induced Monolayer Altermagnetism in $\text{MnP}(\text{S},\text{Se})_3$ and FeSe (2023), arXiv:2309.02355 [cond-mat.mes-hall].
- [67] Y. Zhu, T. Chen, Y. Li, L. Qiao, X. Ma, C. Liu, T. Hu, H. Gao, and W. Ren, Multipiezo Effect in Altermagnetic V_2SeTeO Monolayer, *Nano Letters* **24**, 472 (2024).
- [68] R. Jaeschke-Ubiergo, V. K. Bharadwaj, T. Jungwirth, L. Šmejkal, and J. Sinova, Supercell altermagnets, *Phys. Rev. B* **109**, 094425 (2024).
- [69] D. Go, D. Jo, H.-W. Lee, M. Kläui, and Y. Mokrousov, Orbitronics: Orbital currents in solids, *Europhysics Letters* **135**, 37001 (2021).
- [70] D. Jo, D. Go, G.-M. Choi, and H.-W. Lee, Spintronics meets orbitronics: Emergence of orbital angular momentum in solids, *npj Spintronics* **2**, 19 (2024).